Heterogeneous photochemistry of imidazole-2-carboxaldehyde: HO₂ radical formation and aerosol growth

Laura González Palacios[1,2], Pablo Corral Arroyo[3,4], Kifle Z. Aregahegn[6,7], Sarah S. Steimer[3,5,8], Thorsten Bartels-Rausch[3], Barbara Nozière[6], Markus Ammann[3,5], Christian George[6] and Rainer Volkamer[1,2]

[1]{University of Colorado, Department of Chemistry and Biochemistry, 215 UCB, Boulder, CO, 80309, USA}

[2]{University of Colorado, Cooperative Institute for Research in Environmental Sciences (CIRES), 216 UCB, Boulder, CO, 80309, USA}

[3]{Paul Scherrer Institute, Laboratory of Radio- and Environmental Chemistry, 5232 Villigen PSI, Switzerland}

[4] {University of Bern, Department of Chemistry and Biochemistry, 2012 Bern, Switzerland}

[5] {Swiss Federal Institute of Technology Zurich, Institute for Atmospheric and Climate Science, 8092 Zürich, Switzerland}

[6]{Université Lyon 1; Centre National de la Recherche Scientifique (CNRS), UMR5256, IRCELYON, Institut de recherches sur la catalyse et l'environnement de Lyon, F-69626 Villeurbanne, France}

[7]{now at: Chemistry Department, University of California, Irvine, California, 92697-202 }

[8]{now at: University of Cambridge, Department of chemistry, Cambridge CB2 1EW, UK}

Correspondence to: R. Volkamer (rainer.volkamer@colorado.edu).

Abstract

The multiphase chemistry of glyoxal is a source of secondary organic aerosol (SOA), including its light-absorbing product imidazole-2-carboxaldehyde (IC). IC is a photosensitizer that can contribute to additional aerosol ageing and growth when its excited triplet state oxidizes hydrocarbons (reactive uptake) via H-transfer chemistry. We have conducted a series of

27 photochemical coated-wall flow tube (CWFT) experiments using films of IC and citric acid (CA),

28 an organic proxy and H-donor in the condensed-phase. The formation rate of gas-phase HO_2

29 radicals (P_{HO2}) was measured indirectly by converting gas-phase NO into NO_2. We report on

30 experiments that relied on measurements of NO_2 formation, NO loss and HONO formation. P_{HO2}

31 was found to be a linear function of (1) the [IC]×[CA] concentration product, and (2) the photon

32 actinic flux. Additionally, (3) a more complex function of relative humidity ($25\% < RH < 63\%$),

33 and of (4) the O_2/N_2 ratio ($15\% < O_2/N_2 < 56\%$) was observed, most likely indicating competing

34 effects of dilution, HO_2 mobility and losses in the film. The maximum P_{HO2} was observed at 25-

35 55% RH and at ambient O_2/N_2. The HO_2 radicals form in the condensed-phase when excited IC

36 triplet states are reduced by H-transfer from a donor, CA in our system, and subsequently react

37 with O_2 to re-generate IC, leading to a catalytic cycle. OH does not appear to be formed as a

38 primary product but is produced from the reaction of NO with HO_2 in the gas phase. Further, seed

39 aerosols containing IC and ammonium sulfate were exposed to gas-phase limonene and NO_x in

40 aerosol flow tube experiments, confirming significant P_{HO2} from aerosol surfaces. Our results

41 indicate a potentially relevant contribution of triplet state photochemistry for gas-phase HO_2

42 production, aerosol growth and ageing in the atmosphere.

43

44 **1. Introduction**

45 The sources and sinks of radicals play an important role in the oxidative capacity of the

46 atmosphere. Radicals and other oxidants initiate the chemical degradation of various trace gases,

47 which is key in the troposphere (Jacob, 1999). The hydroxyl (OH) and peroxyl (HO_2) radicals

48 belong to the HO_x chemical family and are primarily generated by ultraviolet radiation

49 photochemical reactions (Calvert and Pitts, 1966), like the reaction of $O(^1D)$ (from O_3) with H_2O,

50 or photolysis of HONO, HCHO, H_2O_2, or acetone. Some secondary gas-phase sources are the

51 ozonolysis of alkenes or $O(^1D) + CH_4$ (Monks, 2005). The oxidation of VOCs by OH and other

52 oxidants in the presence of NO leads to perturbations in the HO_x, NO_x, and RO_x radical cycles that

53 affect O_3 and aerosol formation (Monks, 2005; Sheehy et al., 2010). The kinetics and

54 photochemical parameters of these reactions are relatively well-known in the gas-phase (Atkinson

55 et al., 2004; Sander et al., 2011). However, this does not apply to the sources and sinks for HO_x

56 in atmospheric droplets and on aerosol surfaces (Ervens et al., 2011). Uptake of OH from the gas-

57 phase, and H_2O_2 photolysis in the condensed phase are the primary known sources for HO_x in the

58 condensed-phase. HO_2 is highly soluble and the concentrations of OH, the most effective oxidant

59 in the condensed phase, depend on HO_2 radicals. Another source of HO_x radicals is from the

60 chemical reactions of reduced metal ions and H_2O_2, known as Fenton reactions (Fenton, 1894;

61 Deguillaume et al., 2005). Direct photolysis of H_2O_2, nitrite, nitrate (Zellner et al., 1990),

62 hydroperoxides (Zhao et al., 2013), and light absorbing secondary organic aerosol (SOA) (Badali

63 et al., 2015) are also sources of HO_x in the condensed-phase. Other studies have shown that the

64 photochemistry of iron (III) oxalate and carboxylate complexes, present in aqueous environments

65 (e.g. wastewater, clouds, fogs, particles), can initiate a radical chain reaction serving as an aqueous

66 source of HO_2 and Fe^{2+}. Fe^{2+} can then regenerate OH starting a new cycle of Fenton reactions

67 (Weller et al., 2013a, 2013b). The temperature dependent rate constants of OH in the aqueous

68 phase have been studied for a limited subset of organics (Ervens et al., 2003). However, there is

69 still a wide gap with respect to understanding the sources, sinks, kinetics and photochemical

70 reaction pathways of HO_x radicals in the condensed phase (George et al., 2015).

71 Our study investigates photosensitizers as an additional HO_x source that may be relevant to further

72 modify RO_x and NO_x reaction cycles in both the condensed- and gas-phases. It is motivated by

73 the formation of superoxide in terrestrial aqueous photochemistry (Draper and Crosby, 1983;

74 Faust, 1999; Schwarzenbach et al., 2002), by more recent observations that irradiated surfaces

75 containing titanium dioxide generate HO_x radicals in the gas-phase (Yi et al., 2012) and by the

76 generation of OH from metal oxides acting as photocatalysts in mineral dust (Dupart et al., 2012).

77 Past studies have demonstrated the reactivity of glyoxal towards ammonium ions and amines as a

78 source for light-absorbing brown carbon (Nozière et al., 2009; Galloway et al., 2009; Shapiro et

79 al., 2009; Kampf et al., 2012). One of these products is imidazole-2-carboxaldehyde (IC)

80 (Galloway et al., 2009), which absorbs light at UV wavelengths ($\lambda < 330$ nm) (Maxut et al., 2015).

81 Other imidazole-type compounds and light-absorbing products are formed in minor amounts but

82 can nonetheless impact optical and radiative properties of SOAs (Sareen et al., 2010; Trainic et

83 al., 2011). Photochemical reactions by these species are not typically accounted for in models yet,

84 but have a possible role for SOA formation and aerosol aging mechanisms (Sumner et al., 2014).

85 Photosensitizers are light absorbing compounds that absorb and convert the energy of photons into

86 chemical energy that can facilitate reactions, e.g., at surfaces or within aerosols (George et al.,

87 2015). For example, aerosol seeds containing humic acid or 4-(benzoyl)benzoic acid (4-BBA),

88   two other known photosensitizers, can induce the reactive uptake of VOCs when exposed to light,

89   leading to secondary organic aerosol (SOA) formation (Monge et al., 2012). Aregahegn et al.

90   (2013) and Rossignol et al. (2014) suggested a mechanism for autophotocatalyic aerosol growth,

91   where radicals are produced from the reaction of an H-donor hydrocarbon species, in this case

92   limonene, and the triplet state of IC. The condensed-phase citric acid and the gas-phase limonene

93   are H-atom donors (in this article we refer to them as H-donor), rather than proton donors as is the

94   case of a Brønsted acid. In particular, the transfer of the H-atom leads to the formation of an alkyl-

95   radical species. The H-atoms transfer thus has the same effect as an H-atom abstraction reaction

96   by Cl or OH radicals.

97   Field measurements on fog water samples confirmed that triplet excited states of organic

98   compounds upon irradiation can oxidize model samples such as syringol (a biomass burning

99   phenol) and methyl jasmonate (a green leaf volatile), accounting for $30 - 90\%$ of their loss (Kaur

100 et al., 2014). There are very few field measurements of imidazoles; a recent study by Teich et al.

101 2016 identified five imidazoles (1-butylimidazole, 1-ethylimidazole, 2-ethylimidazole, IC and

102 4(5)-methylimidazole in ambient aerosols in concentrations ranging from 0.2 to 14 ng/m^3. IC, the

103 molecule of interest in this study, was measured in its hydrated form in ambient aerosols in three

104 urban areas with signs of air pollution and biomass burning (Leipzig, Germany, Wuqing and

105 Xianghe, China). The observed quantities of hydrated IC ranged from 0.9 to 3.2 ng/m. The authors

106 claim that these values could be a lower limit due to high losses of IC during sample preparation

107 indicated by low recovery from standard solutions. This suggests that IC and other imidazole

108 derivatives are present in areas with high pollution and biomass burning. Field measurements in

109 Cyprus during the CYPHEX campaign in 2014 detected IC and bis-imidazole in ambient aerosol

110 samples (Jakob, Ronit, 2015). The IC diurnal cycles showed the highest concentrations at night

111 (0.02 – 0.115 ng/m3), and lower concentrations during the day, suggesting that ambient

112 concentrations of IC in aerosols are a balance between photochemical sources and sinks. While

113 imidazoles seem to be widespread in polluted and remote areas, the atmospheric implications of

114 IC, and possibly other photosensitizers related to brown carbon light absorption as radical sources

115 in ambient aerosols is another motivation to conduct this study.

116 The existence of such photocatalytic cycles could be of atmospheric significance. Canonica et al.

117 (1995) suggested indeed that the initial carbonyl, triggering the photochemical properties, is

118 regenerated via a reaction with oxygen producing HO$_2$. To our knowledge, the production of such

119   radical side products was not investigated under atmospheric conditions previously. We therefore

120   report here on the HO_2 radical production from IC in the condensed-phase.

121

2. Experimental Section

123   A series of flow tube experiments were conducted to investigate the formation of gas-phase HO_2

124   radicals from IC photochemistry using two different CWFT reactors (Sect. 2.1). Section 2.2

125   describes aerosol flow tube experiments that confirm the photochemical production of HO_2

126   radicals in the absence of other known gas-phase radical sources in aerosols.. All experiments were

127   performed at atmospheric pressure.

2.1. Coated-wall flow tube experiments

129   The CWFT experiments were designed to investigate the gas-phase production of HO_2 radicals

130   from a film containing IC and citric acid (CA) matrix as a function of UV light intensity, IC

131   concentration in the film, relative humidity (RH), and O_2 mixing ratio. Two similar experimental

132   setups were used as shown in Fig. 1. Some of the differences, not major, consist in the flow reactor

133   volume, surface area, flow rates, IC mass loading, NO mixing ratio, temperature inside the reactor

134   and the connected instrumentation.

135   **Setup 1.** Experiments were conducted in a photochemical flow-system equipped with a Duran

136   glass CWFT (0.40 cm inner radius, 45.2 and 40.0 cm length, inner surface = 113.6 and 100.4 cm^2,

137   S/V = 5.00 cm^{-1}), which was housed in a double jacketed cell coupled to a re-circulating water

138   bath to control the temperature at 298 K; The setup is shown in Fig. 1A. A thin film of IC+CA was

139   deposited inside the tubular glass flow tube. The experimental procedure for the preparation of

140   the films is described in Sect. 2.1.2. The system consisted of seven ultraviolet lamps (UV-A range,

141   Philips Cleo Effect 22 W: 300-420 nm, 41 cm, 2.6 cm o.d.) surrounding the flow tube in a circular

142   arrangement of 10 cm in diameter.

143   **Setup 2.** The second CWFT (CWFT 0.60 cm inner radius, 50 cm length, inner surface 188.5 cm^2,

144   S/V = 3.33 cm^{-1}) reactor had a glass jacket to allow water to circulate and maintain temperature

145   control inside the tube at 292 K. The coated-wall tubes were snuggly fit into the CWFT as inserts.

146   The CWFT was surrounded by the same seven fluorescent lamps as in Setup 1. The light passed

147   through different circulating water cooling jackets for both setups, thus providing a different light

148   path for each setup.

149   **Setup 1 and 2.** The actinic flux in the flow tube reactor, $F_{FT}(\lambda)$, was measured by actinometry of

150   NO$_2$ (see Supplement for description of J_{NO2} measurements), independently for both setups. The

151   flows of N$_2$, O$_2$, air and NO were set by mass flow controllers. The RH was set by a humidifier

152   placed after the admission of N$_2$ and O$_2$ gases but before the admission of NO or NO$_2$ (see Fig. 1),

153   in which the carrier gas bubbles through liquid water at a given temperature. The humidifier could

154   also be by-passed to set a RH of near zero. A typical measurement sequence is described in Sect.

155   2.1.2.

156   The J_{NO2} was measured for both Setup 1 and 2 using NO$_2$ actinometry. The J_{NO2} with seven lamps

157   was found to be 2×10^{-2} s^{-1} for Setup 1 and 1×10^{-2} s^{-1} for Setup 2 (see Fig. S1 for Setup 1, and

158   Supplemental Information text for both Setups). These values were compared to direct irradiance

159   measurements in the flow tube and thus normalized (see Sect. 3.1.1).

160

2.1.1. Flow tube instrumentation

162   The following gas-phase products exiting the flow tube were measured by three different

163   instruments: NO$_2$ by the University of Colorado Light Emitting Diode Cavity-Enhanced

164   Differential Optical Absorption Spectroscopy (LED-CE-DOAS) instrument (Thalman and

165   Volkamer, 2010), HONO by a LOng Path Absorption Photometer (LOPAP, QuMA Gmbh,

166   Heland, J., 2001; Kleffmann et al., 2002), and NO by a chemiluminescence analyzer (Ecophysics

167   CLD 77 AM, also used for NO$_2$ in Setup 2). HO$_2$ radicals were indirectly measured by detecting

168   NO$_2$ with the LED-CE-DOAS (Setup 1) and by the loss of NO with the chemiluminescence

169   detector (Setup 2). The latter was preceded by a molybdenum converter to transform HONO and

170   NO$_2$ to NO, and by an alkaline trap for HONO. Both, trap and converter, had a bypass to allow

171   sequential measurements and thereby obtaining the concentration of NO$_2$ and HONO separately.

172   HONO was measured by the LOPAP during some selected experiments (Kleffmann et al., 2002,

173   2006).

LED-CE-DOAS

The LED-CE-DOAS instrument (Thalman and Volkamer, 2010) detects NO_2 absorption at blue wavelengths. A high power blue LED light source (420–490 nm) is coupled to a confocal high finesse optical cavity consisting of two highly reflective mirrors (R = 0.999956) peaking at 460 nm that are placed about 87.5 cm apart (sample path length of 74 cm). The absorption path length depends on wavelength, and was about ~11 km near peak reflectivity here. A purge flow of dry nitrogen gas is added to keep the mirrors clean. The light exiting the cavity is projected onto a quartz optical fiber coupled to a Princeton Instruments Acton SP2156 Czerny-Turner imaging spectrometer with a PIXIS 400B CCD detector. The mirror reflectivity was calculated by flowing helium and nitrogen gas, exploiting the difference in the Rayleigh scattering cross sections of both gases as described in Thalman et al. (2014). The gas exiting the flow tube was directly injected into the CE-DOAS cavity, and spectra were recorded every 60 seconds, and stored on a computer. For analysis we use BBCEAS fitting at NO_2 concentrations exceeding few ppbv (Washenfelder et al., 2008) and DOAS least squares fitting methods at lower concentrations (Thalman et al., 2015). The mirror alignment was monitored online as part of every spectrum by observing the slant column density of oxygen collision complexes, O_2-O_2 (O_4) (Thalman and Volkamer, 2010, 2013). The following reference spectra were taken from the literature: NO_2 (Vandaele et al., 2002) and O_2-O_2 collision complexes (Thalman and Volkamer, 2013b). The detection limit for NO_2 was 50-100 pptv.

2.1.2. Experimental conditions

The IC+CA solutions were prepared by adding IC into a 1 M CA solution in 18 MΩ ultra-pure water to achieve IC to CA molecular ratios between 0.026 to 0.127 in the film. The bulk solutions for both setups were prepared by weighing out 384-400 mg of CA in 2 mL of water and adding 4-20 mg of IC to the solution. The solutions for both setups were freshly prepared for each experiment and the masses in the film were calculated at 50% RH from the CA hygroscopic growth factors reported by Zardini et al., 2008 for both setups (for Setup 1: 5-18 mg of IC and 44 mg of CA, for Setup 2: 1-5 mg of IC and 77 mg of CA). The range of concentrations in the films was between 0.148 – 0.671 M of IC and 5.29 – 6.68 M of CA.

The IC+CA solution coatings were produced by depositing 220-250 µL (Setup 1) and 400 µL (Setup 2) of the desired solution in a Duran glass tube, which was then dispersed into a thin and

204   viscous film of $3-4\,\mu m$. The film was dried with a gentle N_2 stream humidified to a RH similar

205   to the experimental RH and room temperature. The film was rolled and turned upside down to

206   deposit a homogenous film throughout the entire inner surface of the flow tube. The homogeneity

207   of the film was confirmed by visual inspection. If a bright clear homogenous amorphous film from

208   the super-cooled solution was not observed, the film was discarded (e.g. observation of a turbid

209   and cracked crystallized appearance). The carrier gas flows consisted of premixed dry N_2 and O_2

210   (a ratio of 4.5/1 in Setup 1 and a ratio of 2 in Setup 2), and NO controlled by mass flow controllers.

211   The total flow rates were: 500 mL/min for Setup 1 and 1500 mL/min for Setup 2. In Setup 1, a

212   dilution flow of 1000 mL/min was added at the end of the flow tube for a total of 1500 mL/min

213   during experiments when HONO was measured along with NO_2. All experiments were conducted

214   at ambient pressure, leading to gas residence times of $2.1-2.4$ s (depending on flow tube volume,

215   for both setups) under laminar flow conditions. The O_2 flow rate was varied between 0-110

216   mL/min to observe the dependence of O_2 while keeping the total flow rate constant. A ratio of

217   4.5:1 of N_2:O_2 was maintained if any of the other gas flows were changed (e.g. NO, and/or NO_2)

218   for Setup 1. For Setup 2, a ratio of 2:1 of N_2:O_2 was also maintained, except for the O_2

219   concentration dependence studies. The RH was kept constant at 50% RH during most experiments,

220   and varied between 10-60% RH to study humidity effects of the HO_2 radical production. The

221   concentration of NO was ~1 ppmv (Setup 1) and varied between 100 and 500 ppbv (Setup 2).

222   Scavenging of HO_2 was achieved by the following reaction:

$$NO + HO_2 \rightarrow NO_2 + OH \tag{R1}$$
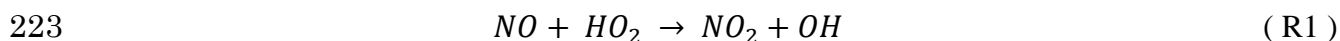
224   The lifetime of HO_2 is about 5 ms when 2.5×10^{13} molecules cm^{-3} of NO are present (Setup 1),

225   which assures efficient conversion of HO_2 molecules into NO_2 ($k = 8.0 \times 10^{-12}$ cm^3 molecule^{-1} s^{-1}

226   at 298 K, Sander et al., 2011). As shown in Fig. S2, 500 ppbv NO, the concentration used in Setup

227   2, was sufficient to efficiently convert HO_2 into NO_2, see Sect. 3.1.1. The lifetime of gas phase

228   HO_2 with respect to loss to the organic film is about 0.1 s, based on a similar formula shown in

229   Equation S3, where $\gamma = 10^{-3}$ (upper limit by Lakey et al., 2015). Note that in view of the essentially

230   diffusion controlled loss of HO_2 to the CWFT and tubing walls, the chosen scheme for determining

231   the production of HO_2 radicals from the films by fast scavenging with NO is superior to a more

232   selective detection method, e.g. LIF, which would require passing the HO_2 radicals into a separate

233   setup with substantial losses. For selected experiments, the films were exposed to UV irradiation

234 for over six hours which showed only a minor change in the decrease of NO_2 concluding the
235 stability of the reactivity of the films.

2.1.3. J_{IC} calculations

237 The absorption cross section of IC and the calculated photolysis rate are shown in Fig. S3. The
238 photolysis frequencies of IC were calculated using a similar procedure as described in
239 Schwarzenbach et al. (2002). The spectral irradiance in the flow tube system was interpolated to
240 the surface area of the flow tube to calculate the spectral photon flux density and the absorbed
241 photon flux:

242 $$F_a^{IC} = \int_{300}^{420} F \times [1 - 10^{-\sigma_{IC}(\lambda) \times b \times C_{IC}}]d\lambda, \qquad \text{where } F = \frac{F_{FT}(\lambda) \times SA}{N_a \times V_{film}}, \qquad (1)$$

243 Where F_a^{IC} is the mean absorbed photon flux in Ein L^{-1} s^{-1} nm^{-1} (1 Ein = 3.0×10^5 J per mole of
244 photons at 400 nm), F is the spectral flux density that reaches the film in the flow tube in moles L^{-1}
245 ^{1} s^{-1} nm^{-1}, b is the optical path length taken as the thickness of the film and C_{IC} is the concentration
246 of IC in the film, and σ_{IC} is the IC absorption cross section. The absorption spectrum of IC in
247 water was based on the measurements by Kampf et al. (2012), and re-normalized to the peak value
248 of 10205 ± 2400 M^{-1} cm^{-1} at 284 nm (Maxut et al., 2015). V_{film} is the volume of the film calculated
249 from the deposited mass of CA and the hygroscopic growth factors of CA (Zardini et al., 2008),
250 SA is the surface area of the flow tube of the film, taken as the geometric area of the inner surface
251 area of the flow tube in cm^2, N_a is Avogadro's number in molecules $mole^{-1}$. The IC photoexcitation
252 rate J_{IC} was about 1.0×10^{-3} s^{-1} (upper limit).

253 We have also attempted to calculate an effective quantum yield for the formation of gas-phase
254 HO_2 radicals (ϕ_{HO2}):

255 $$P_{HO2} = \frac{[NO_2] \times flow}{N_a \times V_{film}} \qquad\qquad \phi_{HO2} = \frac{P_{HO2}}{F_a^{IC}} \qquad (2)$$

256 Where P_{HO2} is the HO_2 production rate in mol L^{-1} s^{-1}, F_a^{IC} is the calculated mean absorbed photon
257 flux by IC (Eq. 1), $[NO_2]$ is the gas-phase concentration of NO_2 in molecules cm^{-3} assuming a 1:1
258 ratio to HO_2 conversion, $flow$ is the volumetric gas flow at the temperature in the CWTF and
259 atmospheric pressure in cm^3 s^{-1}, and V_{film} is in L.

2.2. Aerosol flow-reactor experiments

A detailed description of the aerosol flow tube (AFT) is reported elsewhere (Monge et al., 2012; Aregahegn et al., 2013), therefore, only some principles are recalled below. The SOA experiments were conducted in a horizontal, cylindrical, Pyrex, aerosol flow reactor (13 cm i. d., 152 cm length) surrounded by seven UV lamps (Philips CLEO, 80W) with a continuous emission spectrum ranging from 300-420 nm (total irradiance of 3.31×10^{16} photons cm^{-2} s^{-1}). The flow reactor consisted of Teflon stoppers and different flow controllers that maintained the gas/aerosol/UV irradiation contact time between 20-50 minutes. This flow reactor also consisted of an outer jacket that controlled the temperature at 293 ± 2 K by water circulation using a thermostat (Model Huber CC 405).

Seed aerosols (50 nm) were produced by nebulizing a solution (at pH 6) containing ammonium sulfate (AS, 0.95 mM) and IC (1.3 mM), size selected by a DMA, and exposed to gas-phase limonene (500 ppbv) in the aerosol flow reactor. The typical aerosol mass loading in the reactor was 2-3 μg cm^{-3}, corresponding to ~15000 particles cm^{-3} with a starting diameter of 50 nm. As shown by Aregahegn et al. (in 2013), limonene is an efficient H-donor VOC that forms SOA via reactive uptake to IC containing seed aerosol. Due to the excess of limonene, and low seed aerosol surface are the consumption of limonene was below the detection limit. The aerosol growth was measured by means of an Ultrafine Condensation Particle Counter (UCPC) and a Scanning Mobility Particle Sizer Spectrometer (SMPS; both TSI), and similarly to the CWFT experiment, a flow of gaseous NO (from a 1 ppmv cylinder, Linde) was added to the carrier gas, and its conversion to NO_2 monitored by chemiluminescence detector with a detection limit of 0.05 ppbv (ECO PHYSICS CLD 88). Due to the long residence time, the NO_2 concentration is affected by its photolysis in the AFT. As discussed below, P_{HO2} was calculated, in this case, from the growth of the particle diameter measured at the exit of the flow tube; the assumption is that growth was due to reactive uptake of limonene only, and that each limonene forms one HO_2 radical. At 30 ppbv NO, the HO_2 radical lifetime is around 2 sec.

2.2.1. Experimental conditions

The total flow rate in the aerosol flow reactor was between 400 – 1000 ml/min, ensuring laminar flow conditions. The RH was varied between 0 – 50%. The RH of particles in the flow reactor was controlled by saturating the carrier gas via a bubbler containing ultra-pure water (Milli Q, 18

10

290 Mohm). The RH in the flow reactor system was varied by changing the gas flow rates to the
291 bubbler and the temperature of the circulating water jacket of the bubbler. The RH was measured
292 with a humidity sensor (Meltec UFT 75-AT, Germany) at the exit of the flow reactor. The
293 concentrations for the flow tube experiments were the following: 30 ppbv of NO and 500 ppbv of
294 limonene.

295 **2.3. Chemicals**

296 The following chemicals were used without further purification for CWFT studies: IC (97%,
297 Sigma Aldrich), and CA (Sigma Aldrich). For Setup 1, the Duran glass tubes were soaked in a
298 deconex® cleaning solution overnight, the next day they were rinsed with 18 MΩ water (Milli Q
299 Element system). These flow tubes were etched with a 5% hydrofluoric acid solution after the
300 washing procedure and again rinsed with water before any experimental use. The Duran flow
301 tubes for Setup 2 were not initially etched with any acid but stored in a NaOH solution after
302 washing and lastly rinsed with water; Setup 2 later confirmed that the treatment of flow tube with
303 acids affects P_{HO2} by rinsing with HCl and etching with HF solutions.

304 For the aerosol flow-reactor experiments gas-phase limonene was generated from commercially
305 available limonene (Aldrich, 97%) by means of a permeation tube. The following chemicals were
306 used without further purification: IC (97%, Sigma Aldrich) and succinic acid (Sigma Aldrich,
307 ≥99.5%);4-benzoylbenzoic acid (4-BBA, Aldrich 99%) and adipic acid (AA, Aldrich, ≥99.5%)
308 were used to expand the CWFT studies to other photosensitizers.

309

310 **3. Results and Discussion**

311 **3.1. Coated-wall flow tube**
312 The following results represent the light dependent formation of HO_2 indirectly from
313 measurements of NO_2 production and NO loss, measured with setup 1 and 2, respectively. Figure
314 2 shows a time series of NO_2 measured with setup 1 as a function of UV-A light, which confirms
315 the light dependent radical production. This particular film had an IC/CA ratio of 0.026 (0.148M
316 IC and 5.77M CA in the film). An evident increase of NO_2 is observed upon UV irradiation,
317 directly reflecting the light mediated release of HO_2, as shown in reaction (R1). The NO_2 signal

11

318 decreases over time with all seven lamps was a common feature observed in all films; this could
319 be due to HO_2 sinks in the film increasing with time, thus, the system only slowly evolves into a
320 steady state. A small amount of NO_2 (0.5-1.5 ppbv) was observed during experiments that used
321 only CA in absence of IC; therefore, the data in Fig. 2 and all data reported below have been
322 corrected for this NO_2 background, measured routinely in between experiments. Figure 2 also
323 indicates a strong correlation with irradiance, which is further discussed in the context of Fig. 4.
324 For irradiation, humidity and oxygen dependence experiments, each data point represents a
325 separate experiment using a freshly prepared coated film in the flow tube. The uncertainty for
326 experiments was based on the standard deviation of n, the number of experiments. The total
327 uncertainty was $\pm$ 6-27% (propagated error for normalization was $\pm$ 7–29%) for the IC mass
328 loading experiments in Setup 1 and up to a factor of two for the light dependence experiments.
329 The uncertainty in Setup 2 was 10-50%. As discussed earlier, the lifetime of HO_2 in the system
330 was about three orders of magnitude less than the residence time in the flow tube, therefore
331 suggesting that most, if not all, reacted with NO to produce the observed NO_2 (R1). Theoretically,
332 the system was clean of other oxidants such as O_3 (and thus NO_3). The uptake of NO_2 in the film
333 was very small to further produce any nitrate radicals, and the photolysis of NO_2 in the experiments
334 to produce O_3 was insignificant ($< 1\%$). The recombination of NO and O_3 contributes a negligible
335 ($<0.1\%$) NO_2 source under our experimental conditions. RO_2 generation from the reaction
336 between CA and OH from HONO photolysis was also ruled out since it is approximated to account
337 for only 1% of the NO_2 production if we assume every OH from the photolysis reacts with CA.
338 To our knowledge, the direct photolysis of CA to produce any RO_2 radicals has not been observed.
339 Therefore, we believe that HO_2 is the essential oxidant for NO and refer to the measured NO_2 as
340 HO_2 formation.

341 Figure 3 shows that the HO_2 production fluxes, in molecules cm^{-2} min^{-1}, increased with IC mass
342 loading. The CA concentration was kept constant, and results are shown as the product between
343 [IC] $\times$ [CA], since we expect that the production rate of HO_2 is proportional to the concentration
344 of IC, at constant illumination, and that of the potential H-donor, CA. For Setup 1, the HO_2 fluxes
345 were measured as NO_2 mixing ratios, and calculated using the following equation:

$$346 \qquad Fluxes_{HO_2} = \frac{[NO_2] \times flow}{SA} \qquad\qquad (3)$$

347   the description of these parameters have been previously explained (see Sect. 2.1.3). For Setup 2,

348   the HO_2 flux was calculated similarly, but only about half of the observed NO loss was considered

349   to account for the loss of NO via the reaction with OH (see reaction in Supplement R1), meaning

350   that for each HO_2 scavenged two NO molecules were lost. In Figure 3, the data from Setup 1 are

351   represented by the black squares and the data from Setup 2 are represented by the gray circles.

352   Setup 1 measurements were taken at about ~50% RH and at room temperature. Setup 2

353   measurements were taken at 45% RH and at 292 K. Temperature has an effect on the observed

354   gas-phase HO_2 release from the film and thus needs to be accounted for, which is not accounted

355   for in Fig. 3 but it is described in detail in Sect. 3.1.1.

356   Figure 4 shows that the HO_2 production exhibited a linear dependence on the actinic flux for

357   various [IC] $\times$ [CA] molar products. From Sect. 2.1.3, we estimated an experimental ϕ_{HO2} of

358   about 6×10^{-5}, reflecting other probable, unknown quenching processes in our system. Figure 4

359   also shows the formation of HONO from three different IC mass loadings. In all three cases the

360     $HONO:NO_2$ ratio is < 1, confirming HO_2 as a primary product and OH as a secondary product.

361   Figure 5 shows the dependence of HO_2 production observed via the loss of NO (Setup 2) on

362   relative humidity $(0 - 65\%)$. Water partial pressure is an important parameter in the atmosphere

363   and it seems to also have an important effect on the photochemical reactions studied here. At RH

364   below ~10%, and at high RH above ~55%, the yield of HO_2 radicals decreases. The maximum

365   HO_2 radical production is observed at moderate RH $(20 - 55\%)$. This is probably due to a

366   combination of factors. In particular, at low RH the film may become more viscous reducing

367   mobility, and thus the energy transfer within the film. This may decrease the HO_2 yield as shown

368   in Fig. 5. Hinks et al. (2016) observed that the movement of molecules in a viscous film at a low

369   RH is hindered and thus decreases the photochemical reaction rate of secondary organic material.

370   The reduced diffusivity of HO_2 may also increase the residence time in the film and facilitate the

371   self-reaction in the bulk phase: The diffusivity of H_2O in citric acid is in the range of $10^{-7} - 10^{-8}$

372   cm^2s^{-1} at 50% RH. If the HO_2 diffusivity is between a factor of 10 and 100 lower than that of H_2O

373   due to its larger size, 10^{-9} cm^2s^{-1}, the first order loss rate coefficient for diffusion out of the film,

374   D/δ^2, δ denoting the film thickness $(4 \times 10^{-4}$ cm), becomes about $k_D = 10^{-2}$ s^{-1}. From the observed

375   F_{HO2}, the steady state concentration is then about $F_{HO2}/ k_D /\delta = 4 \times 10^{16}$ $cm^{-3} = 10^{-7}$ M. The loss rate

376   coefficient due to HO_2 self-reaction in the condensed phase $(7.8 \times 10^5$ M^{-1} $s^{-1})$ at this concentration

377   would become nearly 0.1 s^{-1}, somewhat higher than that for diffusional loss. Of course these

378 estimates carry a high uncertainty, but indicate that at lower humidity diffusivity gets low enough

379 to effectively reduce the diffusional loss of HO_2 to the gas phase and favor its loss by self-reaction

380 in the condensed phase. The potential presence of condensed phase sinks, such as RO_2, formed

381 from secondary chemistry of oxidized citric acid may add to this uncertainty. Figure S4 shows

382 that bulk diffusion can be neglected since any HO_2 produced below the first couple of micrometers

383 at the top of the film are likely lost to self-reaction in the condensed phase. This supplementary

384 experiment studied the thickness dependence of the films keeping the IC:CA ratio constant. The

385 results show that P_{HO2} increases linearly with thickness up to ~2.5 um, however, after this thickness

386 the film saturates, showing that this must happen at our films that are between $3 - 4$ µm thick. At

387 high RH ($> 55\%$), the amount of water associated with CA dilutes the reactants, and quenching of

388 the excited IC triplet states gains in relative importance, consistent with findings in other studies

389 (Stemmler et al., 2006, 2007; Jammoul et al., 2008). The RH effect can decrease the HO_2

390 production by a factor of 3, compared to the plateau of maximum HO_2 production between $20 -$

391 55% RH.

392 Figure 6 shows the dependence of the HO_2 production based on the observed NO loss on the O_2

393 mixing ratio (Setup 2). The HO_2 production varied by about 20% over the range of conditions

394 investigated. A decrease below 15% O_2 appears to be significant compared to the maximum HO_2

395 production at ~40% O_2, indicating that O_2 is needed for HO_2 formation. Sufficient O_2 dissolves

396 in the aqueous phase to produce HO_2 radicals efficiently at atmospheric O_2 mixing ratios. We

397 assume that at 55% O_2, the quenching of excited IC triplet states by O_2 has an effect on HO_2

398 production. This effect may decrease P_{HO2} based on our results being qualitatively consistent with

399 the observations of decreasing aerosol growth at high O_2 in the autophotocatalytic aerosol growth

400 described in Aregahegn et al. (2013). However, the experimental focus of this study was based on

401 atmospheric O_2 mixing rations and thus we cannot conclude about the HO_2 production at high O_2

402 mixing ratios.

403 In order to test the possibility for excited IC triplet states to react with NO_2 at the surface of the

404 film, experiments were conducted with NO_2. While we did observe that the uptake of NO_2 on

405 irradiated surfaces scaled with light intensity (see Fig. S5) the reactive uptake coefficient of NO_2

406 to produce HONO at the surface is rather small ($< 2.5 \times 10^{-7}$), corresponding to a k_w of 10^{-3} s^{-1} and

407 thus neither a significant loss of NO_2 nor a significant source of HONO. The primary fate of the

408 nitrogen-containing aromatic alkoxy IC radical under atmospheric conditions is reaction with O_2.

409 However, we have not tested alternative quenching reactions of the triplet state, or other pathways
410 of the reduced ketyl radical that do not result into formation of HONO.

3.1.1 Comparison of data sets

412 The experimental conditions probed differ in the actinic flux, NO concentration, temperature, and
413 acidity. Here, we use the dependencies established in Sect. 3.1 to compare results from both setups.
414 The data from Setup 2 were normalized to conditions of Setup 1. The difference in J_{NO2}
415 corresponds to multiplying results from Setup 2 with a factor of 2.0 ± 0.1. HO_2 was measured
416 indirectly by reacting it with NO, and Fig. S2 indicates the minimum NO concentration needed to
417 efficiently scavenge all gas-phase HO_2 is ~460 ppbv of NO, indicating efficient conversion for
418 Setup 1, and a conversion efficiency of ~0.6 for Setup 2. The data from Setup 2 were multiplied
419 by 1.66 ± 0.10 to normalize for the NO conversion efficiency (Fig. S2), and by an additional factor
420 1.25 ± 0.10 to match temperatures. We observed some limited variability depending on whether
421 HF or HCl were used to clean the flow tube prior to experiments. A higher P_{HO2} was observed
422 when cleaning with HF (Setup 1) compared to storing in NaOH and either rinsing with water or
423 HCl (Setup 2); this is accounted by multiplying data from Setup 2 with a factor of 1.25 ± 0.30.
424 Notably, the error of the correction for the cleaning procedure that is propagated here is larger than
425 the correction factor. The effect of the pretreatment of the flow tubes was not systematically
426 studied, and thus remains a primary uncertainty in the comparison. No further correction was
427 applied for slight differences in RH. The overall correction factor amounts to 5.2 ± 1.4, with the
428 error reflecting the propagated uncertainty. This explains most the difference in P_{HO2} between both
429 setups. The normalized results agree within a factor of 2, which is a reasonably good agreement.

3.1.2 Extension to other photosensitizers

431 A limited number of experiments were performed using the CWFT approach, using 4-BBA as a
432 photosensitizer, in presence of 790 ppbv of gaseous limonene (a possible H-donor) and NO. The
433 organic thin film contained an organic acid matrix made of 4-BBA with/without adipic acid (AA).
434 Also in this system a substantial conversion of NO into NO_2 was observed (see Fig. S6). That 4-
435 BBA behaves similar to the IC system demonstrates that the chemistry discussed above can occur
436 on different excited carbonyls. It is interesting to note that this photo-induced conversion, and HO_2
437 production, was observed to be sustained over long times i.e., more than 15 h probably due to the
438 catalytic nature of the underlying chemical cycles. However, a fraction of the IC did get consumed

439   by photolysis reactions that do not form the excited triplet state (observed during overnight
440   experiments). The HO_2 flux for the 4-BBA system was estimated to be 2.77 x 10^{10} molecules cm$^-$
441   ^{2} min^{-1} making the same assumption that each HO_2 molecule reacts with NO to generate an NO_2
442   molecule. The calculation is based on Eq. 3, where it depends on the concentration of NO_2 as well
443   as the surface area and residence time.

444   **3.2. Aerosol Flow Tube**
445   The aerosol flow tube experiments were conducted similarly to the study by Aregahegn et al.
446   (2013), i.e., who demonstrated that in the absence of NO and known gas phase oxidants, seed
447   particles containing IC can initiate SOA growth in presence of a gaseous H-donor (limonene).
448   Figure 7 shows the results from similar experiments when NO was added to the system. No
449   conversion of NO to NO_2 was observed prior to the injection of limonene into the flow tube. The
450   presence of a gaseous H-donor and light clearly initiated a series of photochemical processes,
451   leading to SOA growth and gaseous NO_2 production. However, the quantitative interpretation
452   of these experiments is not straightforward due to efficient radical cycling in the
453   VOC/NO$_x$/light photochemical system, and the lack of a blank experiment that did not contain
454   IC as part of the seed particles. Limitations arise from the much longer residence time, which
455   allows NO_2 to be significantly photolyzed. The J_{NO2} was estimated as ~6.75 x 10^{-3} s^{-1}, and
456   corresponds to a photolysis lifetime of 2.5 minutes, which is smaller than the actual residence
457   time in the flow tube (~40 mins). Secondary chemistry can lead, among others, to ozone
458   production (O_3 lifetime at 500 ppbv limonene is ~7 min), and secondary OH radical formation
459   from the ozonolysis of limonene. Notably, NO$_x$ is not consumed in Fig. 7. The overall effect
460   of this secondary chemistry is an increased SOA growth compared to an experiment without
461   added NO (Aregahegn et al., 2013). As a consequence, the NO_2 yield cannot be used directly
462   to assess P_{HO2} in presence of NO.

463   However, in the absence of NO these secondary processes can largely be avoided, and are
464   reduced at a level where they cannot be identified (Aregahegn et al., 2013). Under such
465   conditions, the particle growth rates presumably carry information about the photosensitizer
466   cycling and subsequent HO_2 production. If we assume one molecule of limonene reacts to
467   produce one HO_2, the volume change of aerosols is proportional to the overall number of HO_2
468   produced. For example, a growth of 15,000 particles cm^{-3} from diameter 51.4 nm to 68.5 nm in 40

16

469   mins (residence time) is equal to P_{HO2} of 1.67×10^{14} molecules cm^{-2} min^{-1}. This should be

470   interpreted as an upper limit for the actual P_{HO2}, because water uptake may also be

471   contributing to the volume growth. However, compared to the CWFT experiments the much

472   higher surface to volume ratio of nanoparticles is expected to enhance the chemical coupling

473   of a gas-phase H-donor and the excited IC triplet state at the aerosol surface. This is at least

474   in part deemed responsible for the two orders of magnitude higher P_{HO2} in the aerosol flow

475   tube compared to the CWFT experiments. Notably, even if ϕ_{HO2} in the aerosol flow tube was

476   two order of magnitude higher than in the CWFT, it is still significantly smaller than unity.

477   **Primary HO$_2$ formation from IC**

478   One of the main advantages of the CWFT is that it operates at much shorter residence time. From

479   Setup 1, we derive a P_{HO2} of 1.76×10^{12} molecules cm^{-2} min^{-1} for IC/CA = 0.1 and $J_{NO2} = 8 \times 10^{-3}$

480   s^{-1}. This corresponds to 2.9×10^4 molecules cm^{-3} s^{-1} once normalized by aerosol surface area

481   (1.18×10^{-6} cm^2 cm^{-3}), and J_{NO2} in the aerosol flow tube. Such a primary radical flux is equivalent

482   to the OH radical production rate resulting from photolysis of ~1 pptv of HONO in the aerosol

483   flow tube. Conversely, a P_{HO2} of 1.67×10^{14} molecules cm^{-2} min^{-1} is equivalent to the OH radical

484   production rate from ~100 pptv HONO in the aerosol flow tube. We conclude that seed particles

485   containing IC contribute significantly (equivalent to 1-100 pptv HONO) to the primary HO_x radical

486   production rate in the aerosol flow tube experiments in the presence of NO (Fig. 7). Primary HO_2

487   radicals formed from IC containing seed particles react rapidly with NO to form OH radicals under

488   the conditions shown in Figure 7. The H-donor species is further expected to form primary RO_2

489   radicals. These primary HO_2 and RO_2 radicals add directly to the conversion of NO into NO_2, and

490   indirectly by driving secondary NO-to-NO_2 conversion from the RO_2/HO_2 radical chain. The

491   aerosol flow tube experiments thus qualitatively confirm the results obtained from macroscopic

492   surfaces, and highlight the potentially important role of surface-to-volume ratio and gaseous H-

493   donors to enhance the relevance of H-donor photochemistry as sources for HO_x/RO_x radicals and

494   SOA.

495   **3.3. Proposed mechanism**

496   A mechanism that can describe the results from the CWFT experiments is shown in Fig. 8. It

497   follows the mechanism first proposed by Canonica et al., in 1995. The primary product in our

498   system is the HO_2 radical, which forms from the reaction between a nitrogen-containing aromatic

17

499   alkoxy IC radical and a ground state oxygen molecule, recycling the IC molecule. The aromatic

500   alkoxy radicals form from the excited triplet state of IC via transfer of an H atom from an H-donor

501   (in our case likely to be CA, or the CA/H_2O matrix). While a fraction of the IC will get consumed

502   by photolysis reactions that do not form the excited triplet state (see Sect 3.1.2.), IC is also

503   continuously produced from multiphase reactions, e.g., of glyoxal (Yu et al., 2011; Kampf et al.,

504   2012; Maxut et al., 2015). Another conclusion is that OH is a secondary product. If OH was a first

505   generation product we would have expected HONO:NO_2 ratios larger than 1:1. A smaller ratio

506   was observed, as shown in Fig. 4, indicating that there was no direct evidence for primary

507   formation of OH radicals. Interestingly, the H-donor species becomes activated as a result of H-

508   abstraction, and can react further to produce organic peroxy radicals, as evidenced by the aerosol

509   flow tube results.

510

511   **4. Atmospheric relevance**

512   The atmospheric relevance of our findings consists of the possible effect of heterogeneous radical

513   sources to modify atmospheric HO_2 radical concentrations, and facilitate aerosol growth and

514   ageing by adding a radical source within aerosol particles. The production of HO_2 from IC

515   photosensitized heterogeneous chemistry is a possible source of gas-phase HO_2 radicals in ambient

516   air. In order to estimate the possible relevance for HO_2 radical concentrations in urban air, we

517   assume P_{HO2} of 2×10^{12} molecules cm^{-2} min^{-1} (IC/CA = 0.1, Setup 1) as a lower limit, and $2 \times$

518   10^{14} molecules cm^{-2} min^{-1} (IC/AS = 0.1, aerosol flow tube) as an upper limit, and typical conditions

519   in Mexico City (i.e., $J_{NO2} = 8 \times 10^{-3}$ s^{-1} at noontime in Mexico City, aerosol surface area = 15 cm^2

520   m^{-3}; Volkamer et al., 2007). The normalized P_{HO2} during noon time in Mexico City ranges from 2

521    $\times 10^5$ to 2×10^7 molecules cm^{-3} s^{-1}. This corresponds to a rate of new HO_2 radical production of

522   4 to 400 pptv/hr HONO around solar noon in Mexico City (Li et al., 2010), where other radical

523   sources produce about 5.9×10^7 molecules cm^{-3} s^{-1} at solar noon (Volkamer et al., 2010). The

524   upper range value suggests that aerosol surfaces can be a significant source of gas-phase HO_x in

525   places like Mexico City. However, the IC molar ratios used here are likely an upper limit compared

526   to ambient aerosols, yet, in principle other brown carbon molecules (i.e. HULIS and/or other

527   imidazole derivatives) may form additional gas-phase HO_2. The heterogeneous HO_2 radical source

528   could further be relatively more important in unpolluted regions under biogenic influences, where

18

529 gas-phase radical production rates are lower. A more comprehensive characterization of the
530 heterogeneous HO_2 source effect on gas-phase HO_2 radical concentrations hence deserves further
531 investigation.

532 OH radical uptake from the gas-phase is a primary OH source in aerosols (Ervens and Volkamer,
533 2010). Assuming a gas-phase OH concentration of 10^6 molecules cm^{-3}, 15 cm^2 m^{-3} aerosol surface
534 area, and γ_{OH} of unity, the rate of OH uptake is approximately 2.3×10^5 molecules cm^{-3} s^{-1}. The
535 above estimated P_{HO2} is a result from H-transfer to form organic peroxy radicals which is
536 comparable to the rate of OH uptake. The two similar estimates of HO_x suggest that IC is a
537 significant source of radicals in the condensed phase of particles. This is a lower limit due to the
538 unknown radical losses of HO_x to the condensed phase, which hold potential to leverage the HOx
539 source by up to a factor 10,000 if limited by the IC excitation rate. The unknown amount of HO_2
540 that remains in the condensed-phase is a further source of OH in the same phase; this OH, in the
541 presence of reduced metals, can trigger a cycle of Fenton reactions or other oxidizing pathways
542 that can further age the aerosol.

543 These results show that IC, and other aromatic carbonyl photosensitizers, are likely a relevant
544 radical source in aerosol particles. Photo-induced radical generation in condensed phases is
545 currently not represented in atmospheric models that describe aerosol ageing, and warrant further
546 study.

547

548 **5. Conclusion**

549 Three different experimental setups consistently show that HO_2 radicals are produced from the
550 photochemistry of IC in a $CA+H_2O$ matrix and in seed aerosols containing ammonium sulfate (in
551 presence of a gas-phase H-donor, limonene). The linear correlations of P_{HO2} (with [IC]/[CA] and
552 irradiation) yielded maximum P_{HO2} under atmospherically relevant irradiation, O_2 and RH, but
553 also revealed a complex role of film viscosity, and possibly acidity effects (a systematic study of
554 the effect of pH on the IC and CA absorption cross-sections and the product yields from the IC
555 photochemistry is desirable). If the H-donor species is in the condensed phase, significant amounts
556 of HO_2 reach the gas-phase only for moderately high RH (~25 – 55% RH) that facilitates H-
557 transfer, and allows molecules (IC, HO_2) to move freely towards the surface of the film. When
558 the film was too dry this mobility is inhibited due to enhanced viscosity and significantly decreases

559   the P_{HO2}. At RH and O_2 higher than 55%, we observe a decrease in P_{HO2} probably due to dilution

560   by water and competing quenching reactions in the film. We know from Zardini et al. (2008) that

561   pure citric acid does not efflorescence and thus the film remains homogenous in its aqueous phase

562   under all RH conditions. This supports our conclusion that the P_{HO2} is RH dependent since it is

563   partially controlled by the diffusivity in the film. On the contrary, if the H-donor species is in the

564   gas-phase, significant HO_2 production is also observed under dry conditions. The primary fate of

565   the IC•-OH radical at the surface is reaction with O_2 to form HO_2. NO_2 reactions do not appear to

566   form HONO at the surface. Our results suggest that the radical source from photosensitizers such

567   as IC can help jump-start photochemistry of VOCs. The effect on the gas-phase HO_2 radical

568   concentration increases for higher surface to volume ratio of aerosols, and in the presence of gas-

569   phase H-donors. The autophotocatalytic growth of aerosols containing photosensitizers via H-

570   donor chemistry is a SOA source also in the presence of NO, and adds oxidative capacity inside

571   aerosol particles. Further research on other types of H-donors and photosensitizers is necessary to

572   compare different P_{HO2} and rates of aerosol growth from reactive uptake of VOC that could

573   potentially have a significant atmospheric relevance for SOA formation and heterogeneous aerosol

574   ageing.

575   **Author contributions**

576   M.A. and R.V. designed the experiments at PSI; C.G. and B.N. those at IRCELYON. L.G.P.,

577   P.C.A., and K.Z.A. conducted the measurements, analyzed data, and contributed equally to this

578   work. S.S.S., T.B.R. helped during the experiments, and all co-authors contributed to the data

579   interpretation. L.G.P. and R.V. prepared the manuscript with contributions from all co-authors.

580

References

Aregahegn, K. Z., Nozière, B. and George, C.: Organic aerosol formation photo-enhanced by the formation of secondary photosensitizers in aerosols, Faraday Discuss., 165(0), 123–134, doi:10.1039/C3FD00044C, 2013.

Atkinson, R., Baulch, D. L., Cox, R. A., Crowley, J. N., Hampson, R. F., Hynes, R. G., Jenkin, M. E., Rossi, M. J. and Troe, J.: Evaluated kinetic and photochemical data for atmospheric chemistry: Volume I - gas phase reactions of Ox, HOx, NOx and SOx species, Atmos Chem Phys, 4(6), 1461–1738, doi:10.5194/acp-4-1461-2004, 2004.

Badali, K. M., Zhou, S., Aljawhary, D., Antiñolo, M., Chen, W. J., Lok, A., Mungall, E., Wong, J. P. S., Zhao, R. and Abbatt, J. P. D.: Formation of hydroxyl radicals from photolysis of secondary organic aerosol material, Atmos Chem Phys, 15(14), 7831–7840, doi:10.5194/acp-15-7831-2015, 2015.

Calvert, J. G. and Pitts, J. N.: Photochemistry, Wiley, New York., 1966.

Canonica, S., Jans, U., Stemmler, K. and Hoigne, J.: Transformation Kinetics of Phenols in Water: Photosensitization by Dissolved Natural Organic Material and Aromatic Ketones, Environ. Sci. Technol., 29(7), 1822–1831, doi:10.1021/es00007a020, 1995.

Deguillaume, L., Leriche, M., Desboeufs, K., Mailhot, G., George, C. and Chaumerliac, N.: Transition metals in atmospheric liquid phases: sources, reactivity, and sensitive parameters, Chem. Rev., 105(9), 3388–3431, doi:10.1021/cr040649c, 2005.

Draper, W. M. and Crosby, D. G.: Photochemical generation of superoxide radical anion in water, J. Agric. Food Chem., 31(4), 734–737, doi:10.1021/jf00118a014, 1983.

Dupart, Y., King, S. M., Nekat, B., Nowak, A., Wiedensohler, A., Herrmann, H., David, G., Thomas, B., Miffre, A., Rairoux, P., D'Anna, B. and George, C.: Mineral dust photochemistry induces nucleation events in the presence of SO2, Proc. Natl. Acad. Sci. U. S. A., 109(51), 20842–20847, doi:10.1073/pnas.1212297109, 2012.

Ervens, B., Gligorovski, S. and Herrmann, H.: Temperature-dependent rate constants for hydroxyl radical reactions with organic compounds in aqueous solutions, Phys. Chem. Chem. Phys., 5(9), 1811–1824, doi:10.1039/b300072a, 2003.

Ervens, B., Turpin, B. J. and Weber, R. J.: Secondary organic aerosol formation in cloud droplets and aqueous particles (aqSOA): a review of laboratory, field and model studies, Atmos Chem Phys, 11(21), 11069–11102, doi:10.5194/acp-11-11069-2011, 2011.

Faust, B. C.: Aquatic Photochemical Reactions in Atmospheric, Surface, and Marine Waters: Influences on Oxidant Formation and Pollutant Degradation, in Environmental Photochemistry, edited by D. P. Boule, pp. 101–122, Springer Berlin Heidelberg. [online] Available from: http://link.springer.com/chapter/10.1007/978-3-540-69044-3_4 (Accessed 7 December 2015), 1999.

622 Fenton, H. J. H.: LXXIII.?Oxidation of tartaric acid in presence of iron, J. Chem. Soc. Trans., 65,
623 899, doi:10.1039/ct8946500899, 1894.

624 Galloway, M. M., Chhabra, P. S., Chan, A. W. H., Surratt, J. D., Flagan, R. C., Seinfeld, J. H.
625 and Keutsch, F. N.: Glyoxal uptake on ammonium sulphate seed aerosol: reaction products and
626 reversibility of uptake under dark and irradiated conditions, Atmos Chem Phys, 9(10), 3331–
627 3345, doi:10.5194/acp-9-3331-2009, 2009.

628 George, C., Strekowski, R. S., Kleffmann, J., Stemmler, K. and Ammann, M.: Photoenhanced
629 uptake of gaseous NO2 on solid organic compounds: a photochemical source of HONO?,
630 Faraday Discuss., 130, 195–210; discussion 241–264, 519–524, 2005.

631 George, C., Ammann, M., D'Anna, B., Donaldson, D. J. and Nizkorodov, S. A.: Heterogeneous
632 Photochemistry in the Atmosphere, Chem. Rev., doi:10.1021/cr500648z, 2015.

633 Heland, J., J. K.: A new instrument to measure gaseous nitrous acid (HONO) in the atmosphere.,
634 Environ. Sci. Amp Technol., 35(15), 3207–12, doi:10.1021/es000303t, 2001.

635 Hinks, M. L., Brady, M. V., Lignell, H., Song, M., Grayson, J. W., Bertram, A. K., Lin, P.,
636 Laskin, A., Laskin, J. and Nizkorodov, S. A.: Effect of viscosity on photodegradation rates in
637 complex secondary organic aerosol materials, Phys. Chem. Chem. Phys., 18(13), 8785–8793,
638 doi:10.1039/C5CP05226B, 2016.

639 Jacob, D.: Introduction to Atmospheric Chemistry, Princeton University Press, Princeton, N.J.,
640 1999.

641 Jakob, Ronit: Entwicklung von chiralen- sowie RP-HPLC- Methoden in Verbindung mit
642 hochaufloesender MS und deren Anwendung zur Analyse sekundaerer organischer Aerosole in
643 der Atmosphaere, Doktor der Naturwissenchaften, Johannes Gutenberg-Universitaet Mainz,
644 Mainz, Germany., 2015.

645 Jammoul, A., Gligorovski, S., George, C. and D'Anna, B.: Photosensitized Heterogeneous
646 Chemistry of Ozone on Organic Films, J. Phys. Chem. A, 112(6), 1268–1276,
647 doi:10.1021/jp074348t, 2008.

648 Kampf, C. J., Jakob, R. and Hoffmann, T.: Identification and characterization of aging products
649 in the glyoxal/ammonium sulfate system – implications for light-absorbing material in
650 atmospheric aerosols, Atmos Chem Phys, 12(14), 6323–6333, doi:10.5194/acp-12-6323-2012,
651 2012.

652 Kaur, R., Anastasio, C., Valsaraj, K. T., Vempati, H. S. and Vaitilingom, M.: Photoformation of
653 Triplet Excited States and Other Oxidants in Fog Waters and Their Impact on Fog Processing of
654 Organic Compounds, AGU Fall Meet. Abstr., 53, 07, 2014.

655 Kleffmann, J., Heland, J., Kurtenbach, R., Lörzer, J. C. and Wiesen, P.: A new instrument
656 (LOPAP) for the detection of nitrous acid (HONO), Environ. Sci. Pollut. Res., 9(4), 48–54,
657 2002.

658 Kleffmann, J., Wiesen, P. and Kern, C.: Intercomparison of the DOAS and LOPAP techniques
659 for the detection of nitrous acid, 2006.

660 Lakey, P. S. J., George, I. J., Whalley, L. K., Baeza-Romero, M. T. and Heard, D. E.:
661 Measurements of the HO2 Uptake Coefficients onto Single Component Organic Aerosols,
662 Environ. Sci. Technol., 49(8), 4878–4885, doi:10.1021/acs.est.5b00948, 2015.

663 Li, G., Lei, W., Zavala, M., Volkamer, R., Dusanter, S., Stevens, P. and Molina, L. T.: Impacts
664 of HONO sources on the photochemistry in Mexico City during the MCMA-2006/MILAGO
665 Campaign, Atmos Chem Phys, 10(14), 6551–6567, doi:10.5194/acp-10-6551-2010, 2010.

666 Maxut, A., Noziere, B., Fenet, B. and Mechakra, H.: Formation Mechanism and yield of small
667 Imidazoles from Reactions of Glyoxal with NH4+ in water at neutral pH, Phys. Chem. Chem.
668 Phys., doi:10.1039/C5CP03113C, 2015.

669 Monge, M. E., Rosenørn, T., Favez, O., Müller, M., Adler, G., Riziq, A. A., Rudich, Y.,
670 Herrmann, H., George, C. and D'Anna, B.: Alternative pathway for atmospheric particles
671 growth, Proc. Natl. Acad. Sci., 109(18), 6840–6844, doi:10.1073/pnas.1120593109, 2012.

672 Monks, P. S.: Gas-phase radical chemistry in the troposphere, Chem. Soc. Rev., 34(5), 376–395,
673 doi:10.1039/B307982C, 2005.

674 Nozière, B., Dziedzic, P. and Córdova, A.: Products and Kinetics of the Liquid-Phase Reaction
675 of Glyoxal Catalyzed by Ammonium Ions (NH4+), J. Phys. Chem. A, 113(1), 231–237,
676 doi:10.1021/jp8078293, 2009.

677 Rossignol, S., Aregahegn, K. Z., Tinel, L., Fine, L., Nozière, B. and George, C.: Glyoxal induced
678 atmospheric photosensitized chemistry leading to organic aerosol growth, Environ. Sci.
679 Technol., 48(6), 3218–3227, doi:10.1021/es405581g, 2014.

680 Sander, S. P., Abbatt, J., Barker, J. R., Burkholder, J. B., Friedl, R. R., Golden, D. M., Huie, R.
681 E., Kolb, C. E., Kurylo, M. J., Moortgat, G. K., Orkin, V. L. and Wine, P. H.: Chemical Kinetics
682 and Photochemical Data for Use in Atmospheric Studies, Evaluation No. 17, JPL Publ. 10-6, Jet
683 Propulsion Laboratory, Pasadena [online] Available from: http://jpldataeval.jpl.nasa.gov, 2011.

684 Sareen, N., Schwier, A. N., Shapiro, E. L., Mitroo, D. and McNeill, V. F.: Secondary organic
685 material formed by methylglyoxal in aqueous aerosol mimics, Atmos Chem Phys, 10(3), 997–
686 1016, doi:10.5194/acp-10-997-2010, 2010.

687 Schwarzenbach, R. P., Gschwend, P. M. and Imboden, D. M.: Environmental Organic
688 Chemistry, 2 edition., Wiley-Interscience, New York., 2002.

689 Shapiro, E. L., Szprengiel, J., Sareen, N., Jen, C. N., Giordano, M. R. and McNeill, V. F.: Light-
690 absorbing secondary organic material formed by glyoxal in aqueous aerosol mimics, Atmos
691 Chem Phys, 9(7), 2289–2300, doi:10.5194/acp-9-2289-2009, 2009.

692 Sheehy, P. M., Volkamer, R., Molina, L. T. and Molina, M. J.: Oxidative capacity of the Mexico
693 City atmosphere – Part 2: A ROx radical cycling perspective, Atmos Chem Phys, 10(14), 6993–
694 7008, doi:10.5194/acp-10-6993-2010, 2010.

695 Stemmler, K., Ammann, M., Donders, C., Kleffmann, J. and George, C.: Photosensitized
696 reduction of nitrogen dioxide on humic acid as a source of nitrous acid, Nature, 440(7081), 195–
697 198, doi:10.1038/nature04603, 2006.

698 Stemmler, K., Ammann, M., Elshorbany, Y., Kleffmann, J., Ndour, M., D'Anna, B., George, C.
699 and Bohn, B.: Light induced conversion of nitrogen dioxide into nitrous acid on submicron
700 humic acid aerosol, Atmospheric Chem. Phys. Discuss., 7, 4035–4064, 2007.

701 Sumner, A. J., Woo, J. L. and McNeill, V. F.: Model Analysis of Secondary Organic Aerosol
702 Formation by Glyoxal in Laboratory Studies: The Case for Photoenhanced Chemistry, Environ.
703 Sci. Technol., 48(20), 11919–11925, doi:10.1021/es502020j, 2014.

704 Teich, M., van Pinxteren, D., Kecorius, S., Wang, Z. and Herrmann, H.: First Quantification of
705 Imidazoles in Ambient Aerosol Particles: Potential Photosensitizers, Brown Carbon
706 Constituents, and Hazardous Components, Environ. Sci. Technol., 50(3), 1166–1173,
707 doi:10.1021/acs.est.5b05474, 2016.

708 Thalman, R. and Volkamer, R.: Inherent calibration of a blue LED-CE-DOAS instrument to
709 measure iodine oxide, glyoxal, methyl glyoxal, nitrogen dioxide, water vapour and aerosol
710 extinction in open cavity mode, Atmos Meas Tech, 3(6), 1797–1814, doi:10.5194/amt-3-1797-
711 2010, 2010.

712 Thalman, R. and Volkamer, R.: Temperature dependent absorption cross-sections of O_2–O_2
713 collision pairs between 340 and 630 nm and at atmospherically relevant pressure, Phys. Chem.
714 Chem. Phys., 15(37), 15371–15381, doi:10.1039/C3CP50968K, 2013.

715 Thalman, R., Zarzana, K. J., Tolbert, M. A. and Volkamer, R.: Rayleigh scattering cross-section
716 measurements of nitrogen, argon, oxygen and air, J. Quant. Spectrosc. Radiat. Transf., 147, 171–
717 177, doi:10.1016/j.jqsrt.2014.05.030, 2014.

718 Thalman, R., Baeza-Romero, M. T., Ball, S. M., Borrás, E., Daniels, M. J. S., Goodall, I. C. A.,
719 Henry, S. B., Karl, T., Keutsch, F. N., Kim, S., Mak, J., Monks, P. S., Muñoz, A., Orlando, J.,
720 Peppe, S., Rickard, A. R., Ródenas, M., Sánchez, P., Seco, R., Su, L., Tyndall, G., Vázquez, M.,
721 Vera, T., Waxman, E. and Volkamer, R.: Instrument intercomparison of glyoxal, methyl glyoxal
722 and NO2 under simulated atmospheric conditions, Atmos Meas Tech, 8(4), 1835–1862,
723 doi:10.5194/amt-8-1835-2015, 2015.

724 Trainic, M., Abo Riziq, A., Lavi, A., Flores, J. M. and Rudich, Y.: The optical, physical and
725 chemical properties of the products of glyoxal uptake on ammonium sulfate seed aerosols,
726 Atmos Chem Phys, 11(18), 9697–9707, doi:10.5194/acp-11-9697-2011, 2011.

727 Vandaele, A. C., Hermans, C., Fally, S., Carleer, M., Colin, R., Mérienne, M.-F., Jenouvrier, A.
728 and Coquart, B.: High-resolution Fourier transform measurement of the NO2 visible and near-

24

729   infrared absorption cross sections: Temperature and pressure effects, J. Geophys. Res.
730   Atmospheres, 107(D18), 4348, doi:10.1029/2001JD000971, 2002.

731   Volkamer, R., San Martini, F., Molina, L. T., Salcedo, D., Jimenez, J. L. and Molina, M. J.: A
732   missing sink for gas-phase glyoxal in Mexico City: Formation of secondary organic aerosol,
733   Geophys. Res. Lett., 34(19), L19807, doi:10.1029/2007GL030752, 2007.

734   Volkamer, R., Sheehy, P., Molina, L. T. and Molina, M. J.: Oxidative capacity of the Mexico
735   City atmosphere – Part 1: A radical source perspective, Atmos Chem Phys, 10(14), 6969–6991,
736   doi:10.5194/acp-10-6969-2010, 2010.

737   Washenfelder, R. A., Langford, A. O., Fuchs, H. and Brown, S. S.: Measurement of glyoxal
738   using an incoherent broadband cavity enhanced absorption spectrometer, Atmos Chem Phys,
739   8(24), 7779–7793, doi:10.5194/acp-8-7779-2008, 2008.

740   Weller, C., Horn, S. and Herrmann, H.: Effects of Fe(III)-concentration, speciation, excitation-
741   wavelength and light intensity on the quantum yield of iron(III)-oxalato complex photolysis, J.
742   Photochem. Photobiol. Chem., 255, 41–49, doi:10.1016/j.jphotochem.2013.01.014, 2013a.

743   Weller, C., Horn, S. and Herrmann, H.: Photolysis of Fe(III) carboxylato complexes: Fe(II)
744   quantum yields and reaction mechanisms, J. Photochem. Photobiol. Chem., 268, 24–36,
745   doi:10.1016/j.jphotochem.2013.06.022, 2013b.

746   Yi, J., Bahrini, C., Schoemaecker, C., Fittschen, C. and Choi, W.: Photocatalytic Decomposition
747   of H2O2 on Different TiO2 Surfaces Along with the Concurrent Generation of HO2 Radicals
748   Monitored Using Cavity Ring Down Spectroscopy, J. Phys. Chem. C, 116(18), 10090–10097,
749   doi:10.1021/jp301405e, 2012.

750   Yu, G., Bayer, A. R., Galloway, M. M., Korshavn, K. J., Fry, C. G. and Keutsch, F. N.: Glyoxal
751   in Aqueous Ammonium Sulfate Solutions: Products, Kinetics and Hydration Effects, Environ.
752   Sci. Technol., 45(15), 6336–6342, doi:10.1021/es200989n, 2011.

753   Zardini, A. A., Sjogren, S., Marcolli, C., Krieger, U. K., Gysel, M., Weingartner, E.,
754   Baltensperger, U. and Peter, T.: A combined particle trap/HTDMA hygroscopicity study of
755   mixed inorganic/organic aerosol particles, Atmos Chem Phys, 8(18), 5589–5601,
756   doi:10.5194/acp-8-5589-2008, 2008.

757   Zellner, R., Exner, M. and Herrmann, H.: Absolute OH quantum yields in the laser photolysis of
758   nitrate, nitrite and dissolved H2O2 at 308 and 351 nm in the temperature range 278-353 K, J.
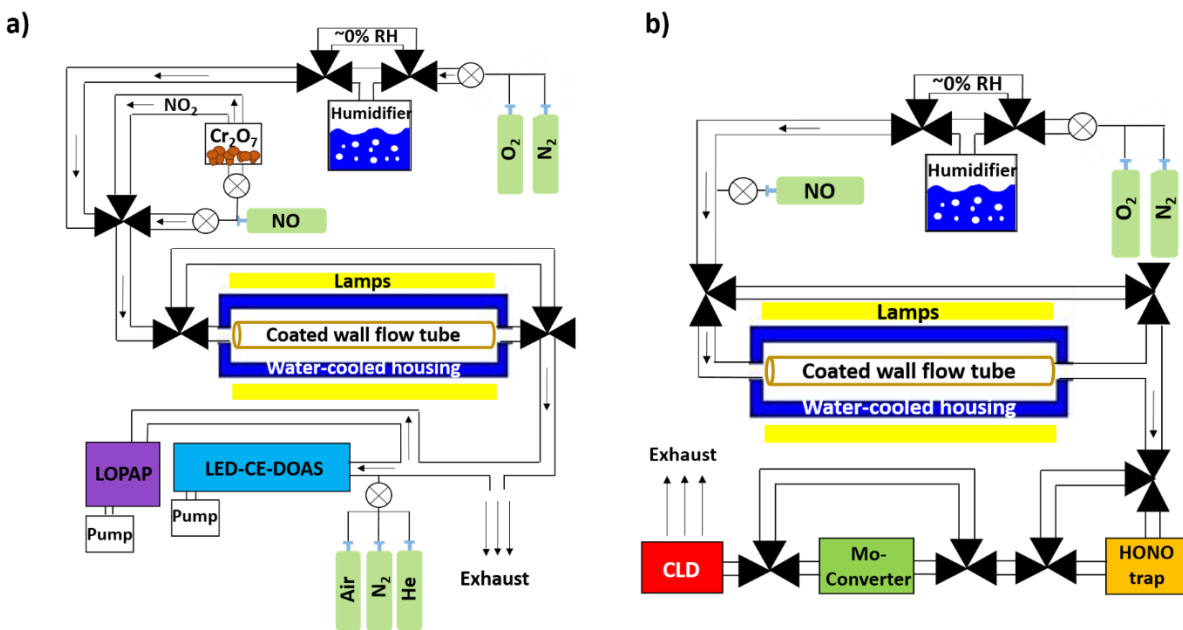759   Atmospheric Chem., 10, 411–425, 1990.

760   Zhao, R., Lee, A. K. Y., Soong, R., Simpson, A. J. and Abbatt, J. P. D.: Formation of aqueous-
761   phase α-hydroxyhydroperoxides (α-HHP): potential atmospheric impacts, Atmos Chem Phys,
762   13(12), 5857–5872, doi:10.5194/acp-13-5857-2013, 2013.
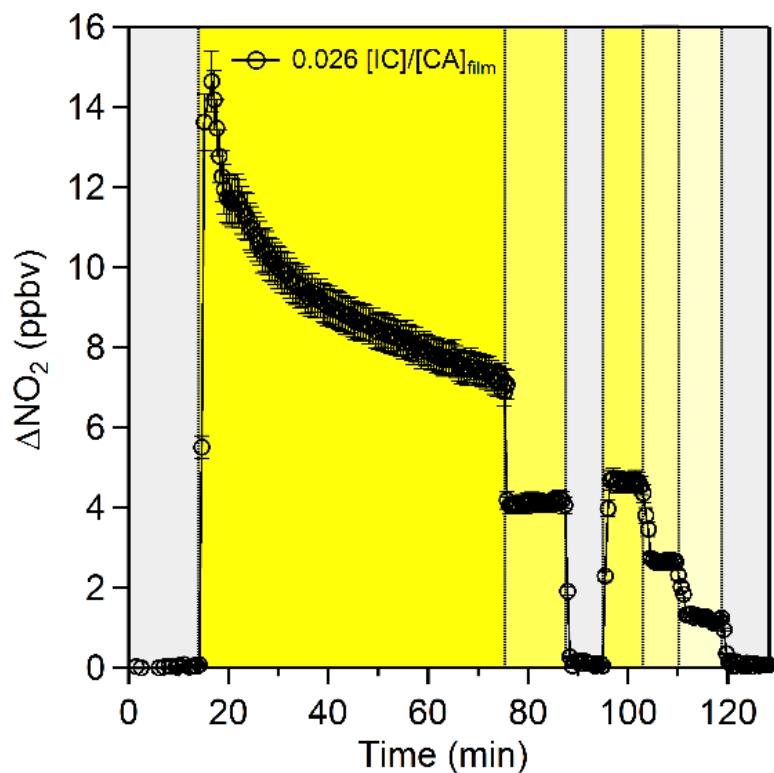
763

764

765

Figures

Figure 1. Sketch of the photochemical flow tube reactor setups at PSI for a) Setup 1 in 2013 measuring NO_2 generation and b) for Setup 2 in 2014 measuring NO loss.

770

771

772

Figure 2. NO$_2$ profile for a 0.025M IC bulk solution, whose concentration increases to ~0.2 M of IC in the film due to the citric acid hygroscopic properties. The gray shaded areas indicate periods where NO was exposed in the dark. The yellow shaded areas indicates the period of irradiation; the decrease in the intensity of yellow represents the decrease in irradiance (2.26 x 10^{16}, 1.47 x 10^{16}, 1.14 x 10^{16}, and 3.94 x 10^{15} photons cm^{-2} s^{-1}, for seven, five, three and one lamp, respectively). This timeseries clearly indicates the light dependence production of HO$_2$ radicals from the photosensitization of IC in a CA film.

780

781

782
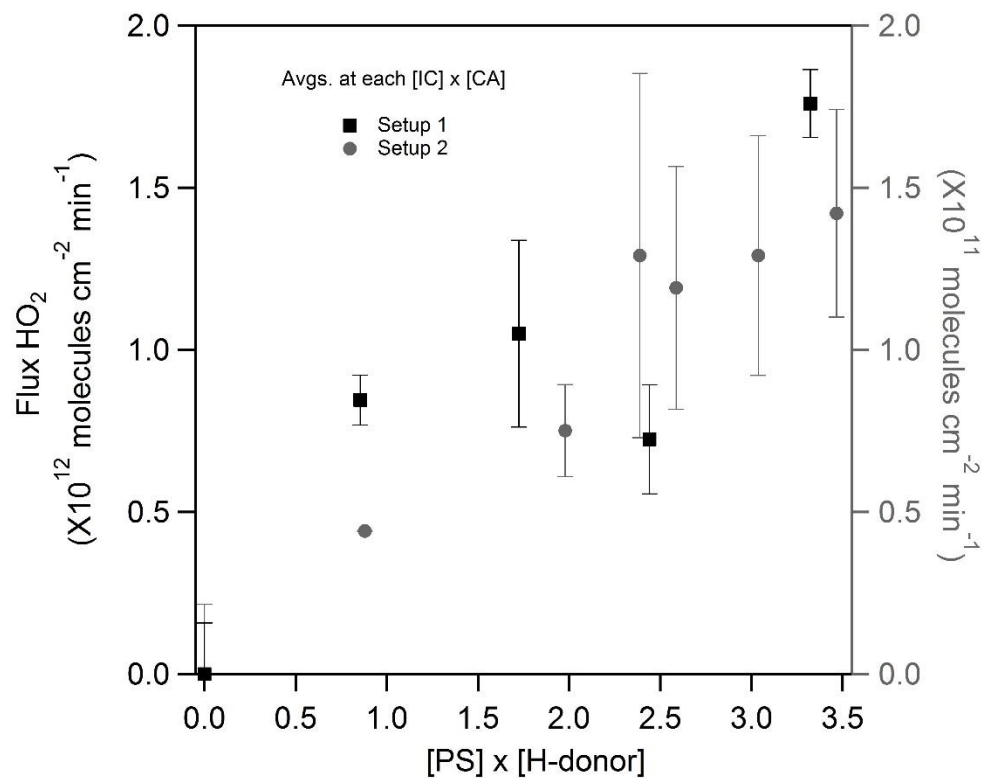
Figure 3. A linear correlation of HO_2 as a function of IC concentration. The left y-axis
represents the values for Setup 1, while the right y-axis represents the values for Setup 2, (an
order of magnitude difference for both scales). The Setup 2 data falls between a factor of 2 and 3
from Setup 1 after accounting for differences between Setup 1 and 2, see Sect. 3.1.1.

787
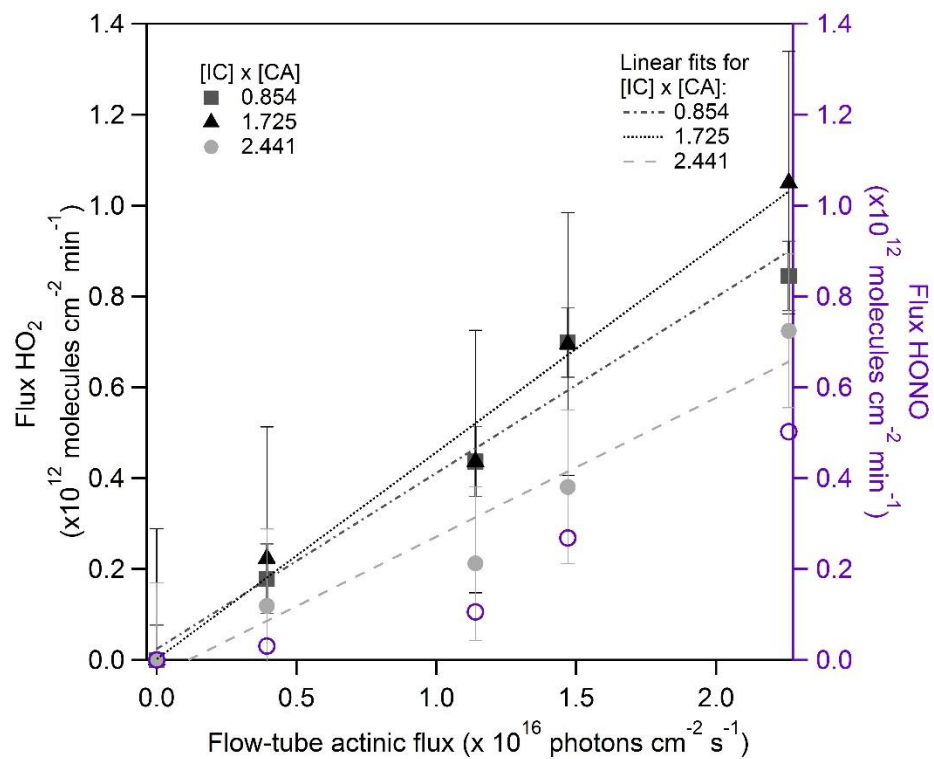
788

789

790   Figure 4. HO_2 fluxes in molecules cm^{-2} min^{-1} as a function of actinic flux for a 300-420 nm range

791   (solid symbols). The data is plotted as a concentration product of [IC] x [CA] (shown in the

792   legend) which shows the photochemical reaction between IC and CA in H_2O matrix and gaseous

793   NO. HONO for 2.441 ([IC] x [CA]) is plotted on the right axis (open circles), showing a ratio of

794   HONO:NO_2 < 1, which suggests OH as a secondary product.

795
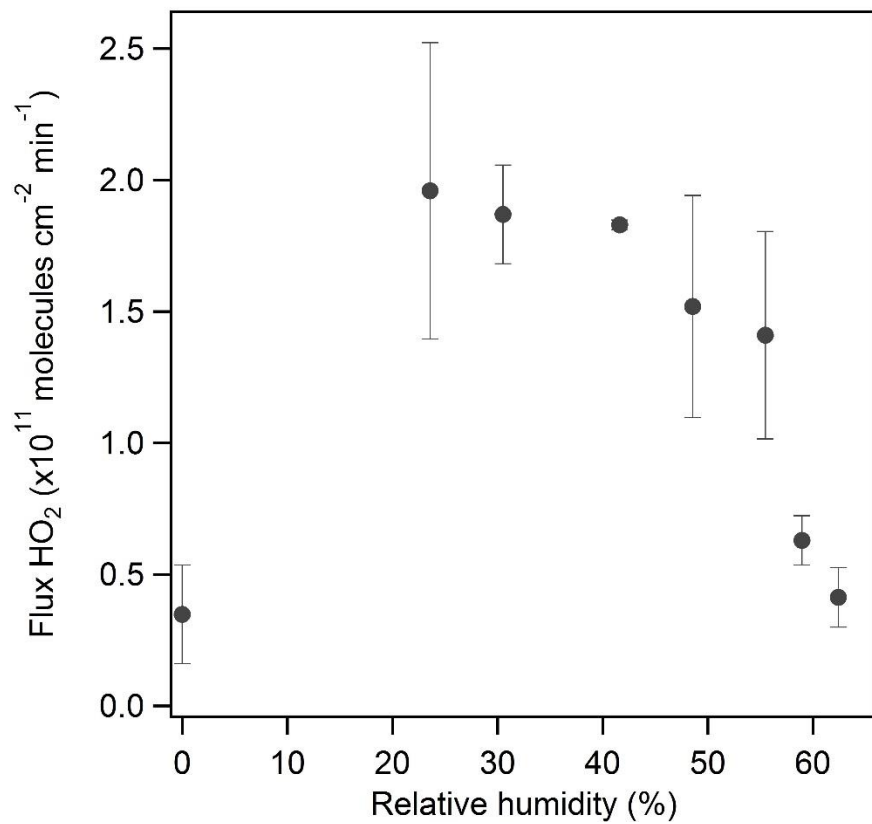
796

797

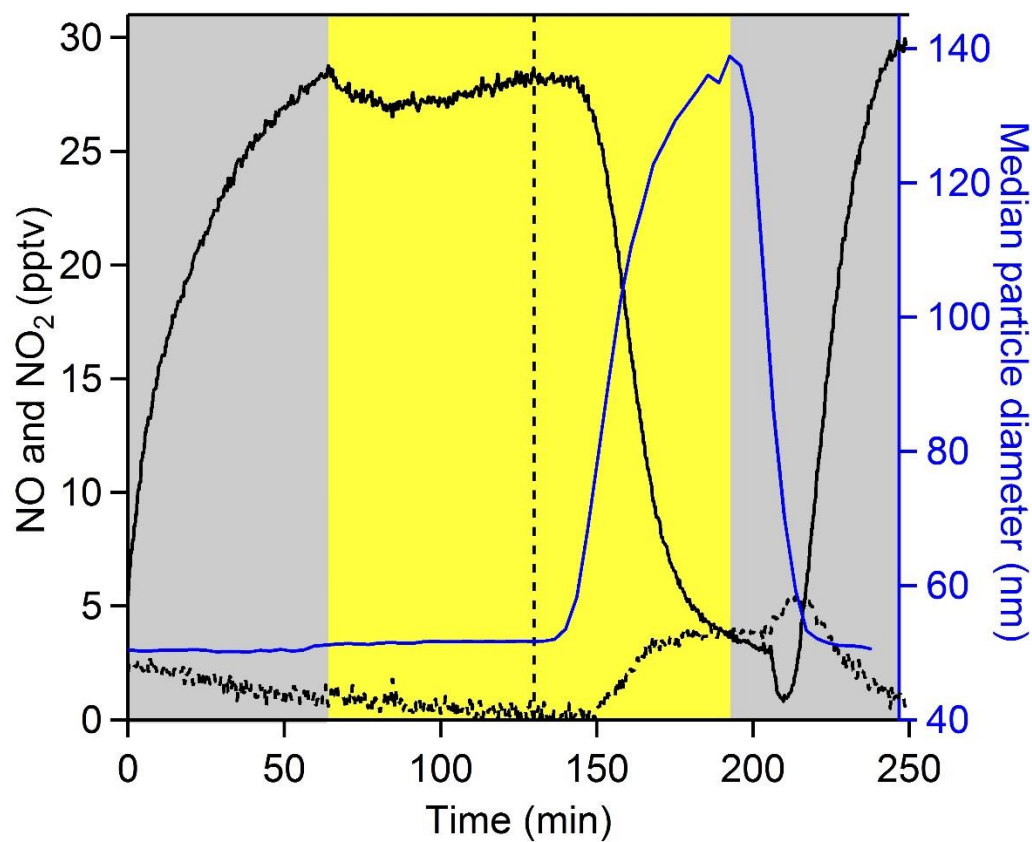798   Figure 5. The NO loss normalized to the film surface area as a function of relative humidity.

799
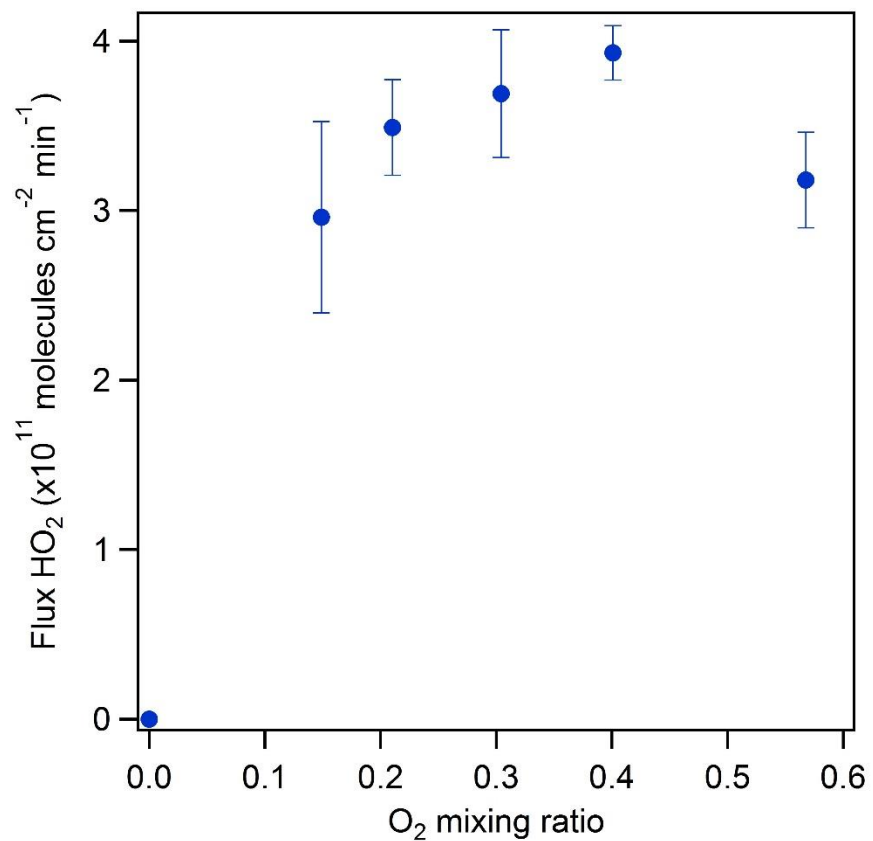
Figure 6. Measured loss of NO above a film composed of IC and CA normalized of the film surface area as a function of the O_2 mixing ratio.

805

806

807   Figure 7. Aerosol flow tube experiments show rapid conversion of NO (solid black line) into

808   NO$_2$ (dashed black line)   only after the time when limonene (gaseous H-donor) is added into the

809   flowtube (vertical dashed line). The gray shaded areas represent experiment in the dark, and the

810   yellow shaded area represents the experiment under light exposure. The blue line represents the

811   growth of aerosols, right axis.

812
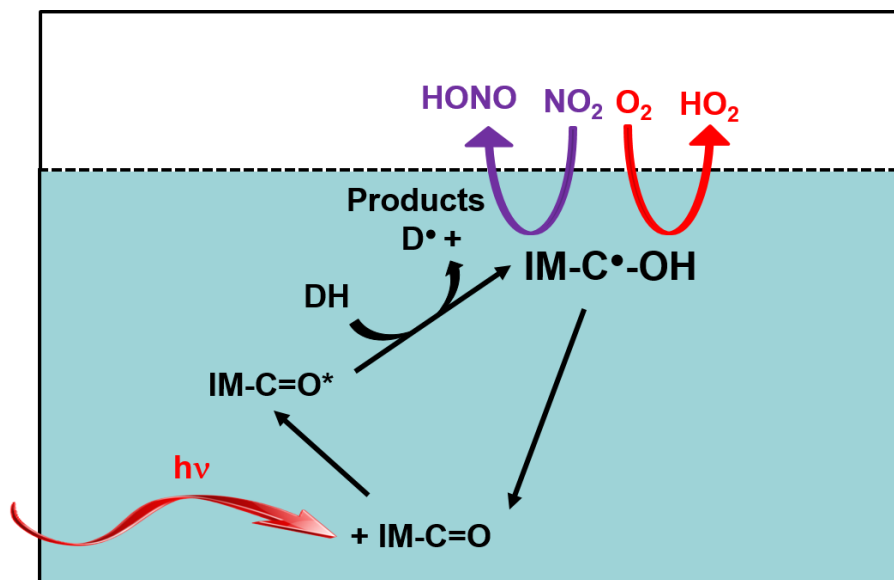
Figure 8. Proposed mechanism, modified and expanded to photosensitization of IC based on Canonica et al. (1995), George et al. (2005) and Aregahegn et al. (2013). The reaction in the white square represents the gas-phase, and the blue square represents the aqueous phase. DH is an H-donor (e.g. CA, another IC, H2O+CA matrix to be determined from flash photolysis).